International Journal of Technology 12(4) 829-842 (2021)
Received January 2021 / Revised May 2021 / Accepted July 2021

International Journal of Technology

http://ijtech.eng.ui.ac.id

Alternative Empirical Formula for Predicting the Frictional Drag Penalty due to Fouling on the Ship Hull using the Design of Experiments (DOE) Method

Muhammad Luqman Hakim[1], Bagus Nugroho[2], I Ketut Suastika[1], I Ketut Aria Pria Utama[1*]

[1]*Department of Naval Architecture, Institut Teknologi Sepuluh Nopember, Surabaya 60111, Indonesia*
[2]*Department of Mechanical Engineering, The University of Melbourne, Victoria 3010, Australia*

Abstract. Biofouling is known as one of the main problems in the maritime sector because it can increase the surface roughness of the ship's hull, which will increase the hull's frictional resistance ($\boldsymbol{\Delta C_F}$) and consequently, the ship's fuel consumption and emissions. It is thus important to reduce the impact of biofouling by predicting the value of $\boldsymbol{\Delta C_F}$. Such prediction using existing empirical methods is still a challenge today, however. Granville's similarity law scaling method can predict accurately because it can be adjusted for all types of roughness using the roughness function $\boldsymbol{\Delta U^+(k^+)}$ variable as the input, but it requires iterative calculations using a computer, which is difficult for untrained people. Other empirical methods are more practical to use but are less flexible because they use only one $\boldsymbol{\Delta U^+(k^+)}$ input. The variance of $\boldsymbol{\Delta U^+(k^+)}$ is very important to represent the biofouling roughness that grew randomly. This paper proposes an alternative formula for predicting the value of $\boldsymbol{\Delta C_F}$ that is more practical and flexible using the modern statistical method, the Design of Experiments (DOE), particularly two-level full factorial design. For each factor, the code translation method using nonlinear regression combined with optimization of constants was utilized. The alternative formula was successfully created and subjected to a validation test. Its error, calculated against the result of the Granville method, had a coefficient of determination $\boldsymbol{R^2}$= 0.9988 and an error rate of ±7%, which can even become ±5% based on 93.9% of 1,000 random calculations.

Keywords: Added frictional resistance; Biofouling; Design of experiments; Empirical formula; Ship resistance

1. Introduction

The impact of fouling or biofouling on ship performance is important (Molland et al., 2014). Biofouling makes the hull's surface rough, and hence, increases its frictional resistance (ΔC_F), which becomes a drag penalty that increases fuel consumption. As a result of biofouling, the fuel consumption could increase by up to 20% (Hakim et al., 2019); in fact, in one year, total losses from fuel waste due to biofouling reached up to $56 million (Schultz et al., 2011). By increasing fuel consumption, biofouling also contributes to increasing CO_2 emissions and global warming. Moreover, biofouling mediates the distribution of invasive species that can damage the water ecosystem structure (Ulman et al., 2019). To prevent these unwanted problems due to biofouling, a more efficient hull may be designed (Sulistyawati and Suranto, 2020) or a more efficient propeller (Abar and Utama, 2019), or

*Corresponding author's email: kutama@na.its.ac.id, Tel.: +62-31-5947254; fax: +62-31-5964182
doi: 10.14716/ijtech.v12i4.4692

a device may be installed (Suastika et al., 2017), but the easiest solution is to predict the impact of biofouling.

When the fluid passes through the rough surface, the turbulence boundary layer structure will be shifted downward. Mathematically, the value of the downward shift can be estimated using what is called a *roughness function* [$\Delta U^+(k^+)$], which is a function of the roughness length scale (k^+). The form of the roughness function varies widely, depending on the type of roughness, including the pattern, density, geometry, and other aspects of the roughness (Chung et al., 2021). To find out accurately the form of the roughness function, the roughness must be tested first (Speranza et al., 2019) by conducting an experiment (Monty et al., 2016), a numerical simulation (Jelly and Busse, 2018; Suastika et al., 2021), or in-situ measurement (Utama et al., 2018). Then, the results of many tests can be synthesized into formulas or diagrams that can be used as an empirical method. As we know, the empirical method is the easiest, fastest, and cheapest method to use as an initial predictive tool.

Each of the existing empirical methods is challenging to use. While the similarity law scaling boundary layer method of Granville (1958, 1987) yields accurate results because it can accommodate all types of roughness by entering the $\Delta U^+(k^+)$ and k of the desired roughness, it requires iterative calculations on a computer, which makes it difficult for untrained people to use. The formula of Bowden and Davison (1974), and the formula of Townsin et al. (1982) and Townsin (2003), calculate ΔC_F easily, but they are applicable to only one type of roughness function [$\Delta U^+(k^+)$]. Besides, for the roughness height parameter, only a single parameter—the average hull roughness (AHR)—is used, whereas in biofouling, the roughness is very random, (especially biofouling), such that the density, shape, and pattern must also be considered to achieve an accurate prediction result (Chung et al., 2021). Finally, the method of reading the diagrams introduced by Demirel et al. (2019) is very easy to use, but if the value being determined is unavailable, it still needs to be interpolated or extrapolated. Moreover, the diagrams accommodate only one type of roughness function, that of Schultz and Flack (2007), when several types of roughness functions are most often used, namely, those of Colebrook (1939), Nikuradse (1933), and their derivatives (Grigson, 1992; Cebeci and Bradshaw, 1977; Schultz and Flack, 2007; Demirel et al., 2017a).

Therefore, this paper proposes an alternative formula for predicting the value of ΔC_F that is easy to use and flexible because it can accommodate several types of $\Delta U^+(k^+)$. This formula was established with the help of the Design of Experiments (DOE) method, which is a branch of modern statistics. The DOE is known to be useful for modeling with small amounts of data and even with many parameters (factors) (Lye, 2002). The type of DOE used in this study was the two-level factorial design with four factors, followed by factor code translations using the nonlinear regression and optimization method. To our knowledge, factor code translations are rarely used. Some statistical software that we often encounter also do not do factor code translations but stop at the result of a formula whose input factor is still a code (-1 or +1), which is not the actual value of the factor. Islam and Lye (2009) predicted the value of the hydrodynamic performance of the propeller without translating the factor code to the actual value, so their resulting formula became difficult to use. Therefore, in this study, we developed a different formula for predicting the impact of biofouling. We tested the result of the formula against the result of the similarity law scaling method of Granville (1958), which was used with iterative calculations. The error rate was calculated from all the error results of 1,000 random calculations.

2. Methods

2.1. Granville's Boundary Layer Similarity Law Scaling

Using the similarity law scaling method of Granville (1958), the boundary layer was extrapolated based on the desired inputs. This method is illustrated in Figure 1. With this method, the value of ΔC_F was calculated using Equations 1–3 by determining the values of L (the ship length), V (the ship speed), and k (the roughness height), and the type of $\Delta U^+(k^+)$, where C_{F_R} is the coefficient of frictional resistance in a rough condition; C_{F_S} is the coefficient of frictional resistance in a smooth condition taken from the approximated Kármán-Schoenherr formula (Schoenherr, 1932); Re is the Reynolds number, which is a function of the L and V of the ship and is calculated as $\rho VL/\mu$; ρ is the fluid density; μ is dynamic viscosity; ${C_{F_S}}'$ is the coefficient of frictional resistance for the new Re that is shifted by $\Delta U^+\kappa[\ln(10)]^{-1}$, κ is the von Kármán constant; k^+ is the roughness Reynolds number; ν is the kinematic viscosity; U_τ is the friction velocity defined as $\sqrt{\tau_w/\rho}$ or approached by $U_\infty(C_F/2)^{1/2}$; τ_w is the shear stress magnitude; and U_∞ is the freestream velocity or is equal to V. To calculate U_τ, the value of C_F is needed, which is equal to the value of C_{F_R}. Although C_{F_R} is what we are calculating, the iteration must be calculated to complete it.

$$\Delta C_F = C_{F_R} - C_{F_S} = C_{F_R} - \frac{0.0795}{(\mathrm{Log}_{10}\mathrm{Re} - 1.729)^2} \tag{1}$$

$$C_{F_R} = {C_{F_S}}' = \frac{0.0795}{\left(Log_{10}\left(\mathrm{Re} - (\Delta U^+\kappa[\ln(10)]^{-1})\right) - 1.729\right)^2} \tag{2}$$

$$\Delta U^+ = f(k^+) = f\left(\frac{kU_\tau}{\nu}\right) \tag{3}$$

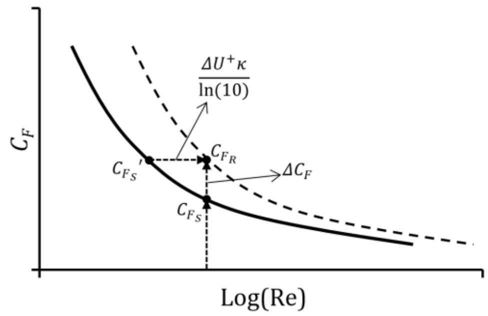

Figure 1 Granville's similarity law scaling method

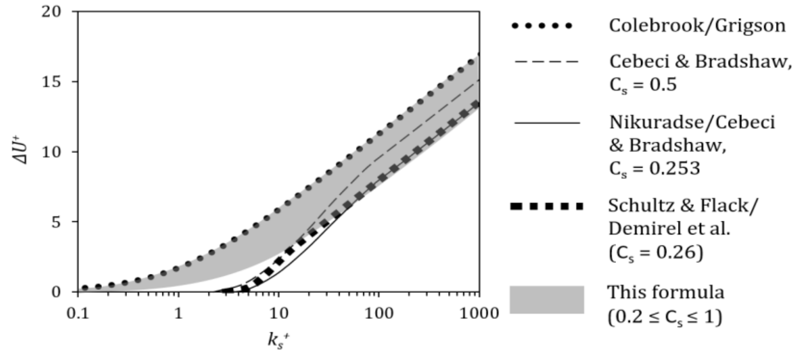

Figure 2 Comparison of some types of roughness functions [$\Delta U^+(k^+)$] with the roughness function used in the proposed alternative formula

2.2. Roughness Functions

Each type of roughness has its characteristic roughness function [$\Delta U^+(k^+)$]. Generally, there are two groups of roughness functions (Andersson et al., 2020): the Colebrook-type (Grigson, 1992) single-expression function ('single regime'; see Equation 4) and the regime with three functions. These three functions are the Cebeci and Bradshaw (1977) roughness function, given as $k^+_{s_{smooth}} = 2.25$; the Nikuradse roughness function (see Equation 5); and the Schultz and Flack (2007) roughness function, that both follow the traditional Nikuradse (1933) roughness function . For the second group of $\Delta U^+(k^+)$, they can be distinguished by the value of the constants described in Equation 5, $k^+_{s_{rough}} = 90$, and $C_s = 0.253$ (for the) or 0.5; Schultz and Flack (2007) roughness function was fitted by Demirel et al. (2017) with $k^+_{s_{smooth}} = 3$, $k^+_{s_{rough}} = 15$, and $C_s = 0.26$. All these types of roughness functions are plotted in Figure 2.

$$\Delta U^+ = \frac{1}{\kappa}\ln(1 + k^+) \tag{4}$$

$$\Delta U^+ = \begin{cases} 0 & \rightarrow \quad k^+ \le k^+_{smooth} \\ \dfrac{1}{\kappa}\ln(C_s k^+)\sin\left(\dfrac{\pi}{2}\dfrac{\ln(k^+/k^+_{smooth})}{\ln(k^+_{rough}/k^+_{smooth})}\right) & \rightarrow \quad k^+_{smooth} \le k^+ \le k^+_{rough} \\ \dfrac{1}{\kappa}\ln(C_s k^+) & \rightarrow \quad k^+ > k^+_{rough} \end{cases} \tag{5}$$

The Colebrook/Grigson-type roughness function has been used in various studies, such as by Yeginbayeva and Atlar (2018) to examine the roughness of some marine coatings with mimicked hull roughness ranges, by Schultz (2004) to analyze Fouled and unfouled coatings, and by Demirel et al. (2017b) to investigate the artificial barnacle. The roughness function of Cebeci and Bradshaw (1977), with C_s = 0.253 and 0.5, corresponds to the roughness of the paints studied by Atencio and Chernoray (2019). The roughness conditions of the typical AF coating and some of the fouling levels were described by the roughness function of Schultz (2007), which corresponds to the roughness functions of Schultz and Flack (2007) and Demirel et al. (2017).

To simplify this study's development of an alternative formula for the roughness function that can accommodate some roughness functions at once, attempts were made to represent some of those roughness functions with similar equations. First, the Colebrook/Grigson-type roughness function (Equation 4) was assumed to have a variable C_s whose value was 1. Then, Equation 4 could be represented by Equation 6, with C_s = 1. Second, the Nikuradse-type roughness function (Equation 5) was used only for the fully rough regime. Therefore, Equation 5 could be approximated only by Equation 6, while keeping C_s, i.e., 0.253, 0.26, and 0.5, variable. As a result, the alternative formula to be proposed will have boundary conditions and error rates especially in fully smooth and transition regimes, as illustrated in Figure 2. The author tolerates this reasoning because the fully rough regime has the greatest impact and thus, needs greater attention than the other regimes. This reason is also reinforced by the Colebrook-type roughness function, which uses only a single regime.

$$\Delta U^+ = \frac{1}{\kappa}\ln(1 + C_s k^+) \tag{6}$$

2.3. Two-level Full Factorial Design

The two-level full factorial design was used to build the alternative formula. Four factors were used, so the number of runs (the data required) was $2^4 = 16$ (Hinkelmann, 2012). The four factors are described in Table 1, with the lowest and highest values assigned to "Low, X = *-1*" and "High, X = **+1**", respectively. The lowest and highest values were selected based on the author's reasonable assumptions of the range of the ship length (L) and the ship speed (V). The k value range was selected based on the fouling condition range in Schultz (2007), and the range of the C_s values was chosen to cover some of the roughness functions described in Subsection 2.2. Regarding the selection range of the C_s values from 0.2 to 1, the author deliberately set the minimum value at 0.2 so as not to be too rigid. Although the smallest value from the review in Subsection 2.2 is 0.253, the author believes that the value of C_s 0.2 can still accommodate the C_s value of 0.253 and 0.26 with good results. However, it is possible to find a certain roughness pattern that matches the roughness function with a C_s value of less than 0.253 or about 0.2. Thus, the alternative formula will be formed as in Equation 7.

Table 1 The factors with their code ($X_{(i)}$) ranges (the low and high values)

	Factors	Label, (i)	Unit	Low, $X_{(i)}$ = *-1*	High, $X_{(i)}$ = **+1**
a	Length of ship	L	m	20	400
b	Ship speed	V	m/s	2	20
c	Fouling condition	k	µm	100	10,000
d	Roughness constant	C_s	-	0.2	1

$$\Delta C_F = f(L, V, k, C_s) \tag{7}$$

Since this was a 2^4 factorial, the ΔC_F data from 16 combinations of the four factors were required. The value of ΔC_F, as $Y_{(i)}$, was calculated and iterated using the Granville method, as described in Section 2.1. The 16 data and the DOE calculations are arranged in Table 2. The combination column explains what factor values were selected as the highest ($X_{(i)}$ = **+1**) or the lowest ($X_{(i)}$ = *-1*). For example, the combination "a" means that the selected input factor for L was +1 or 400 m (see Table 1), while the others were *-1*. In the next example, the combination "acd", where the letter "b" is not mentioned, the factor V that was chosen was *-1* or 2 m/s (see Table 1), while the other factors were **+1**. The ΔC_F data were calculated based on the input of each combination. For the effect values, $\beta_{(0)}$ is the grand mean of all $Y_{(i)}$, while $\beta_{(i)}$ is the average product when $Y_{(i)}$ is multiplied by $X_{(i)}$, which is explained by the sample calculation in Table 3.

After all the effect values were calculated, the initial formula in Equation 9 was created, which was arranged based on Equation 8. The effect is the value of the factor's influence on the result or response, Y or ΔC_F. A positive $\beta_{(i)}$ indicates that the higher the factor or the interaction of the factors is, the higher the response (ΔC_F) is; while a negative $\beta_{(i)}$ means that the higher the factor or the interaction of the factors is, the lower the response (ΔC_F) is.

The Pareto chart was needed to determine which factors or interactions of factors were dominant (see Figure 3). The chart was made based on the absolute value of the effect $\beta_{(i)}$, after which the percentage was calculated. From the chart, it was known that the k factor was the most dominant, with a 1.983 effect, or 30.1%.

Equation 9 is the initial formula that resulted from the two-level full factorial design, which was not final yet, because the factor value that was inputted into the formula was still in the form of a code or $X_{(i)}$. Thus, for example, to input the factor $L = 20$ m, $X_{(L)} = -1$; and if $L = 400$ m, $X_{(L)} = +1$. However, it would not be easy to input the value of $L \neq 20$ m or $L \neq 400$ m. For example, if $L = 100$ m, what is the value of $X_{(L)}$? This problem also occurred

Table 2 The two-level full factorial design matrix and calculation

Combi-nation	Label, (i)	$X_{(i)}$ value							$Y_{(i)}$	Effect
		$X_{(L)}$	$X_{(V)}$	$X_{(k)}$	$X_{(C_s)}$	$X_{(LV)}$	...	$X_{(LVkC_s)}$	$\Delta C_F \times 10^3$	$\beta_{(i)}$
0	0	-1	-1	-1	-1	**+1**	...	**+1**	0.1000	2.583
a	L	**+1**	-1	-1	-1	-1	...	-1	0.0120	-1.144
b	V	-1	**+1**	-1	-1	-1	...	-1	0.7283	0.2465
c	k	-1	-1	**+1**	-1	**+1**	...	-1	4.1033	1.983
d	C_s	-1	-1	-1	**+1**	**+1**	...	-1	0.8985	0.8657
ab	LV	**+1**	**+1**	-1	-1	**+1**	...	**+1**	0.3698	-0.0676
ac	Lk	**+1**	-1	**+1**	-1	-1	...	**+1**	1.6663	-0.9297
ad	LC_s	**+1**	-1	-1	**+1**	-1	...	**+1**	0.4003	-0.445
bc	Vk	-1	**+1**	**+1**	-1	-1	...	**+1**	4.7316	0
bd	VC_s	-1	**+1**	-1	**+1**	-1	...	**+1**	1.5268	0
cd	kC_s	-1	-1	**+1**	**+1**	**+1**	...	**+1**	8.5477	0.569
abc	LVk	**+1**	**+1**	**+1**	-1	**+1**	...	-1	2.0242	0
abd	LVC_s	**+1**	**+1**	-1	**+1**	**+1**	...	-1	0.7581	0
acd	LkC_s	**+1**	-1	**+1**	**+1**	-1	...	-1	2.9609	-0.3425
bcd	VkC_s	-1	**+1**	**+1**	**+1**	-1	...	-1	9.1760	0
$abcd$	$LVkC_s$	**+1**	**+1**	**+1**	**+1**	**+1**	...	**+1**	3.3187	0

Table 3 A sample calculation of the effect, $\beta_{(LkC_s)}$

Label, (i)	1	2	3	4 (1×2×3)	5	6 (4×5)
	$X_{(L)}$	$X_{(k)}$	$X_{(Cs)}$	$X_{(LkC_s)}$	$Y_{(i)}$	$X_{(LkC_s)} \times Y_{(i)}$
0	-1	-1	-1	-1	0.1000	-0.1000
L	**+1**	-1	-1	**+1**	0.0120	0.0120
V	-1	-1	-1	-1	0.7283	-0.7283
...	...	...	...	...	...	...
LkC_s	**+1**	**+1**	**+1**	**+1**	2.9609	2.9609
VkC_s	-1	**+1**	**+1**	-1	9.1760	-9.1760
$LVkC_s$	**+1**	**+1**	**+1**	**+1**	3.3187	3.3187
$\beta_{(\boldsymbol{LkC_s})}$ is the average of the values in column 6 =						-0.3425

$$Y = \beta_{(0)} + \beta_{(L)}X_{(L)} + \beta_{(V)}X_{(V)} + \cdots + \beta_{(LV)}X_{(LV)} + \cdots + \beta_{(LVkC_s)}X_{(LVkC_s)} \tag{8}$$

$$\begin{aligned}\Delta C_F \times 10^3 = {} & 2.583 - 1.144X_{(L)} + 0.2465X_{(V)} + 1.983X_{(k)} + 0.8657X_{(C_s)} \\ & - 0.0676X_{(LV)} - 0.9297X_{(Lk)} - 0.445X_{(LC_s)} + 0.569X_{(kC_s)} \\ & - 0.3425X_{(LkC_s)}\end{aligned} \tag{9}$$

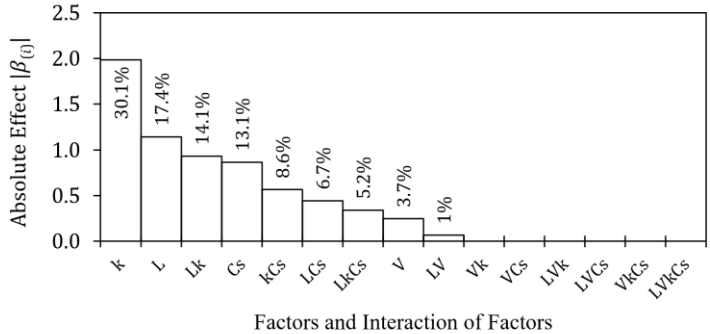

Figure 3 Pareto chart to determine the dominant factor or the interaction of factors

with the other factors. Therefore, the value of $X_{(L)}$ (as a code) was translated into an actual L (un-code). This process is described in Section 2.4.

2.4. Translating the Factor Codes

The next stage was translating the code of factors by knowing the model function of each factor. By knowing the medium value (or midpoint) position, the nonlinearity of each factor was established. The medium values were determined and are shown in Table 4.

The nonlinearity of each factor was discovered by varying the factor and fixing the other factors. For example, the value of L was varied from 20 to 400 m, and the values of V, k, and C_s were made fixed. Based on these combinations, the value ΔC_F was calculated again using the Granville method. After the value of ΔC_F was obtained, it was related to the values of X shown in Table 5 using the iteration method until the best fit between ΔC_F and X values was found. This iteration was assisted by the optimization method, so it was easy to determine the best value with the minimum error. The optimization tool used was a solver prepared in Microsoft Excel based on the Generalized Reduced Gradient (GRG) code (Lasdon et al., 1978). Then, the values of ΔC_F were plotted together with X and L, as shown in Figure 4 (left).

Based on the plotting results for each factor, the form of each factor's function was found using nonlinear regression with the help of the optimization method. To provide an example, the function form of the L factor was obtained with the coefficient of determination $R^2 = 0.9945$. See Figure 4 (left) and Equation 10.

Table 4 The medium code ($X_{(i)}$) values of the factors

Factor	Low ($X_{(i)}$ = -1)	Medium (midpoints) (-1 < $X_{(i)}$ < +1)	High ($X_{(i)}$ = +1)
L	20	31.7; 43.7; 67.5; ...; 352.5	400
V	2	4.2; 6.5; 8.7; ...; 17.7	20
k	100	254.7; 718.8; ...; 8762.5	10000
C_s	0.2	0.3; 0.4; 0.5; ...; 0.9	1

For the other factors, namely, V, k, and C_s, the same procedure as that done for the L factor was followed. Table 6, Figure 4 (right), and Equation 11 provide details of the V factor treatment. Table 7, Figure 5 (left), and Equation 12 show the details for the k factor treatment. Table 8, Figure 5 (right), and Equation 13 show the details for the C_s factor treatment.

Table 5 Calculation of the midpoints of $X_{(L)}$

L (m)	V (m/s)	k (µm)	C_s	$\Delta C_F \times 10^3$	$X_{(L)}$ value	Position
20				5.4229	-1	Low
31.875				4.6122	-0.49	Medium
43.75				4.1559	-0.205	
...	11	5050	0.6	...	...	
305				2.3763	0.91	
352.5				2.2895	0.96	
400				2.2172	1	High

3. Results and Discussion

The alternative formula is shown in Equation 14. It was obtained by combining the initial formula in Equation 9 with each factor's function in Equations 10, 11, 12, and 13.

Table 6 Calculation of the midpoints of $X_{(V)}$

L (m)	V (m/s)	k (µm)	C_s	$\Delta C_F \times 10^3$	$X_{(V)}$ value	Position
	2			2.3107	-1	Low
	4.25			2.4602	-0.25	
	6.5			2.5359	0.12	
210	...	5050	0.6	...	...	Medium
	15.5			2.6743	0.81	
	17.75			2.6940	0.91	
	20			2.7111	1	High

$$X_{(L)} = 1.6577 - 10.426L^{-0.4564} \tag{10}$$

$$X_{(V)} = 4.7874 - 6.5715V^{-0.1836} \tag{11}$$

$$X_{(k)} = 0.1049k^{0.3429} - 1.499 \tag{12}$$

$$X_{(C_s)} = 4.8445{C_s}^{0.3315} - 3.8482 \tag{13}$$

Table 7 Calculation of the midpoints of $X_{(k)}$

L (m)	V (m/s)	k (µm)	C_s	$\Delta C_F \times 10^3$	$X_{(k)}$ value	Position
		100		0.8688	-1	Low
		254.69		1.3102	-0.8	
		718.75		1.9588	-0.5	
50	11	...	0.6	...	...	Medium
		7525		4.6173	0.75	
		8762.5		4.8898	0.88	
		10000		5.1417	1	High

Table 8 Calculation of the midpoints of $X_{(C_s)}$

L (m)	V (m/s)	k (µm)	C_s	$\Delta C_F \times 10^3$	$X_{(C_s)}$ value	Position
			0.2	1.8248	-1	Low
			0.3	2.0877	-0.595	
			0.4	2.2952	-0.27	
210	11	5050	...	...	...	Medium
			0.8	2.8824	0.65	
			0.9	2.9967	0.83	
			1.0	3.1030	1	High

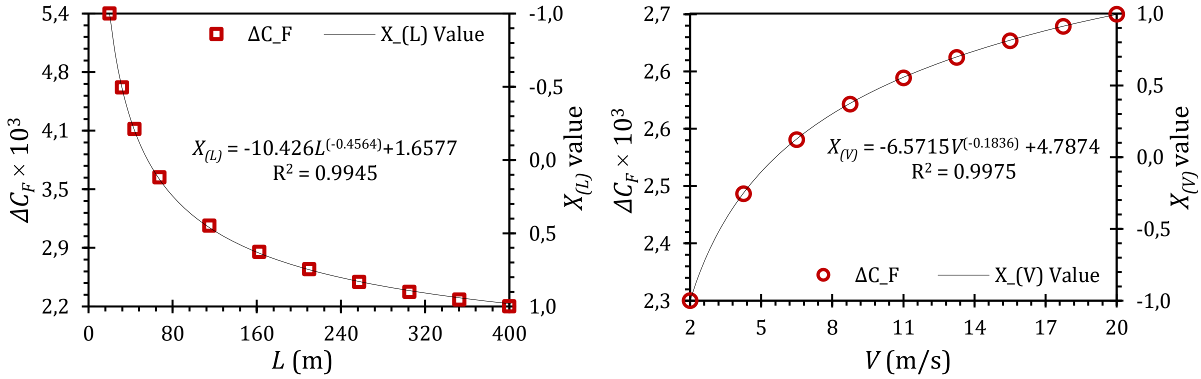

Figure 4 The nonlinear function of $X_{(L)}$ (left) and $X_{(V)}$ (right)

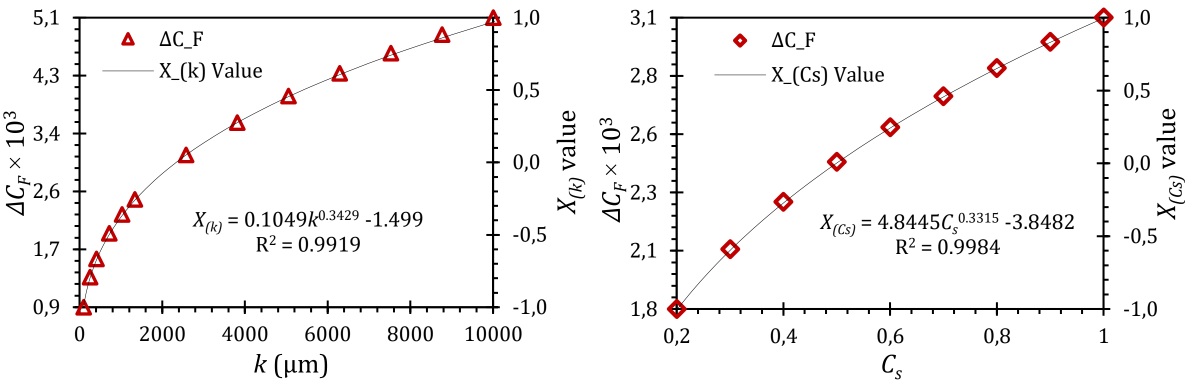

Figure 5 The nonlinear function of $X_{(k)}$ (left) and $X_{(C_s)}$ (right)

The units for each factor were meters (m) for L, m/s for V, and μm for k. C_s was nondimensional.

$$\Delta C_F \times 10^3 = 0.1823 + 3.5167 \cdot L^{-0.4564} - 0.8834 \cdot V^{-0.1836} + 0.0458 \cdot k^{0.3429} + 0.6112 \cdot C_s^{0.3315} - 4.6323 \cdot L^{-0.4564} \cdot V^{-0.1836} - 0.4247 \cdot L^{-0.4564} \cdot k^{0.3429} - 3.4552 \cdot L^{-0.4564} \cdot C_s^{0.3315} + 0.0006 \cdot k^{0.3429} \cdot C_s^{0.3315} + 1.8147 \cdot L^{-0.4564} \cdot k^{0.3429} \cdot C_s^{0.3315} \quad (14)$$

A validation test was performed for this alternative formula to compare the calculation results obtained using this formula with that using the Granville method. The calculation result consisted of 1,000 combinations of factors (L, V, k, and C_s) that were obtained randomly. From the random combination of factors, ΔC_F was calculated using the proposed formula and using the Granville method. The random factors and the calculation results are provided in the supplementary file. The results of the two calculations were compared by plotting them in Figure 6 with the help of linear regression. The test results showed that the coefficient of determination $R^2 = 0.9988$ with $y = 0.9672x + 0.1115$ (red solid line), where the perfect criterion is $y = x + 0$ (black solid line).

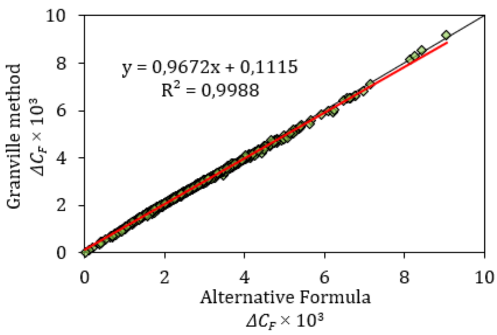

Figure 6 The results of thealternative formula versus the results of the Granville method

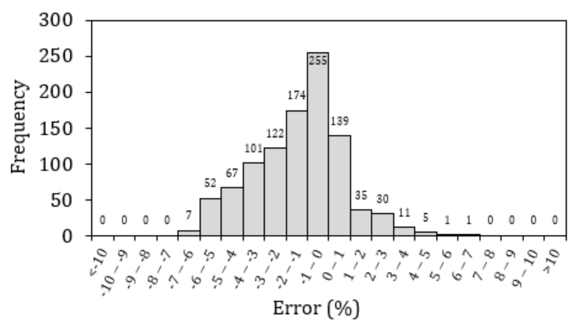

Figure 7 The error distribution of the alternative formula based on the Granville method

The error of this alternative formula based on the Granville method was analyzed to illustrate the confidence level with respect to its accuracy. The error was calculated using Equation 15, after which the error values were arranged in the histogram in Figure 7. The error values were also plotted against the factors in Figures 8 and 9 to show the range of the percentage error risk of each factor value.

$$\text{Error (\%)} = \frac{\Delta C_{F\,(\text{formula})} - \Delta C_{F\,(\text{Granville})}}{\Delta C_{F\,(\text{Granville})}} \times 100\% \tag{15}$$

The error distribution in the histogram (Figure 7) shows that the formula has an error risk of -7% to +5% with 1,000 data and a ±5% error risk if it uses only 93.9% of the 1,000 data. The data distribution shows that the distribution is not symmetrical or is denser on the left (the negative side). This means that many errors occur in negative values (-), which indicates that most predictions using this formula produce values that are slightly smaller than that from the Granville method. However, it should be noted that these values will differ if the amount of data used also differs. In this analysis, it was ensured that the factor values that were used as inputs were varied by as many as 1,000 combinations that were truly randomly generated.

Figures 8 and 9 show that each factor had its own error range, with the red solid line as the centre line value of each data distribution. This can describe the boundary conditions of the proposed formula, so it can predict the risk of calculation error for a certain range of factors. The L factor seems to have had some positive errors (+) when L was less than about 70 m (short), and the most negative errors (-) when L was more than about 70 m [see Figure 8 (left)]. The V factor had a fairly stable error in all its ranges, with all negative errors [see Figure 8 (right)]. Based on Figure 9 (left), the k factor had the largest error at its ranges below about 6,000 µm and even more so in the approximately 1,000µm range. The k factor had less error at the higher values of around 6,000 µm and above. The C_S factor also had less error in the higher value range (more than 0.9).

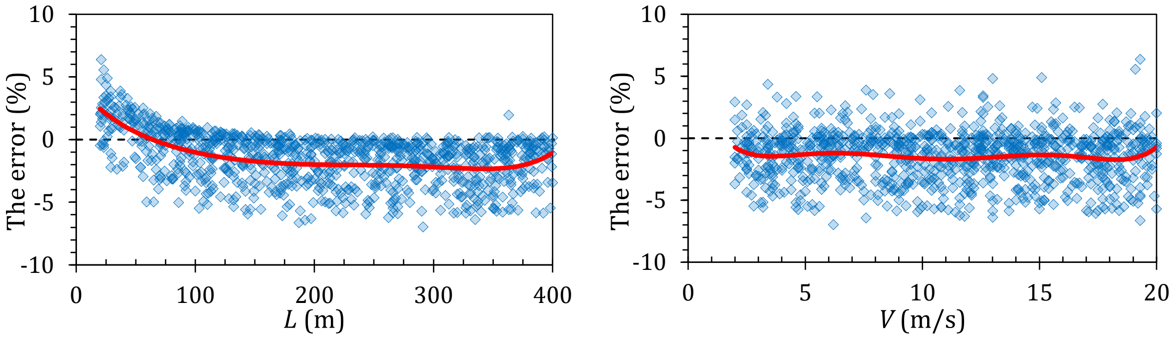

Figure 8 Error distribution based on the L factor range (left) and for the V factor (right)

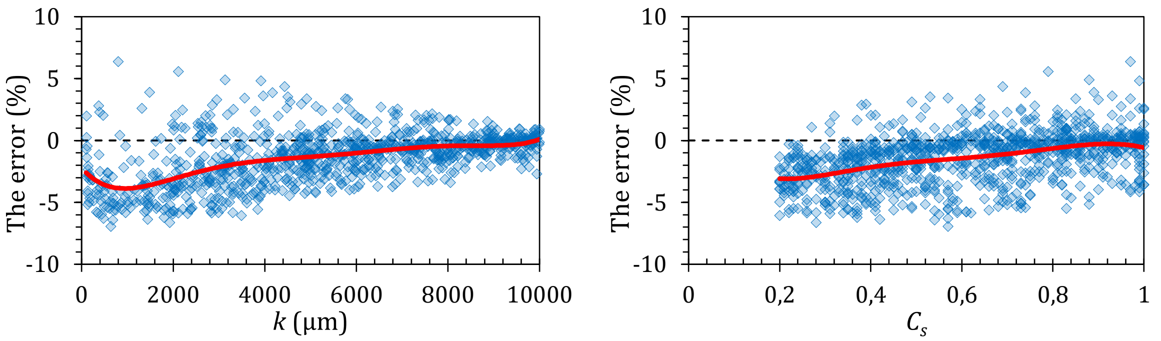

Figure 9 Error distribution values of the k factor range (left) and for the C_S factor (right)

The factors that were used as inputs to the calculation of the response ΔC_F were also analyzed and are shown in Figures 10 and 11. Figure 10 (left) means that ships with a shorter L will be more at risk of experiencing a larger ΔC_F than ships with a longer L. This is consistent with the findings of Hakim et al. (2020). Figure 10 (right) shows that the value of ΔC_F is not too affected by the speed factor (V); but $C_{F_R} = C_{F_S} + \Delta C_F$ denotes, as expected, that faster ships will have greater resistance. That is, ships with any speed will have the same ΔC_F, but will still have different values of C_{F_S}. The worse the fouling condition is, the higher ΔC_F is and vice versa, as shown in Figure 11 (left). According to Figure 11, the higher the roughness constant C_S is, the higher the value of ΔC_F is and vice versa. All the characteristics of the factor effects in this data analysis are in accordance with the predicted effect of the DOE method, which is shown in the Pareto diagram in Figure 3.

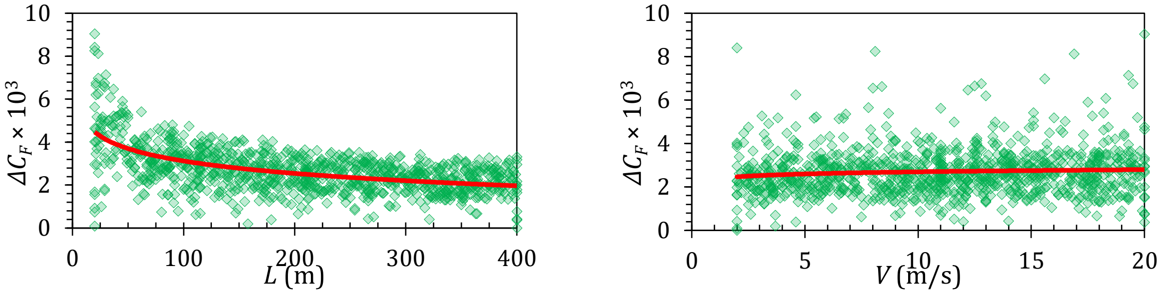

Figure 10 Effect characteristic of the L factor (left) and the V factor (right) to the response ΔC_F

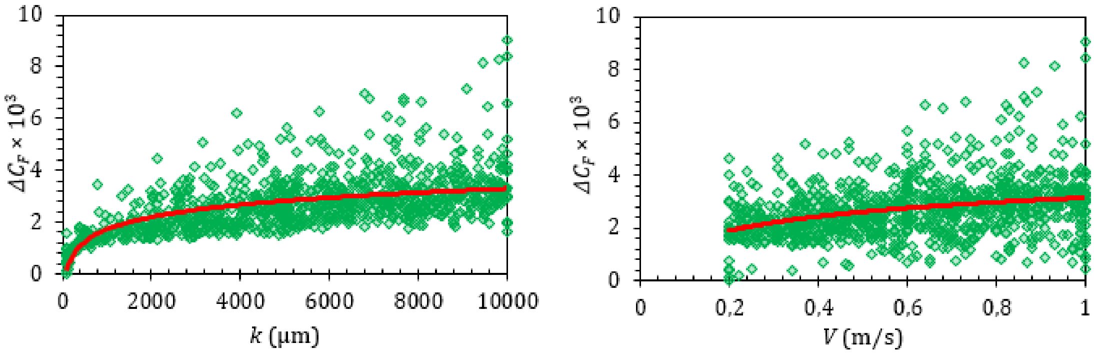

Figure 11 Effect characteristic of the k factor (left) and the C_S factor (right) to the response ΔC_F

4. Conclusions

This paper described the process of establishing an alternative formula for the prediction of the increased frictional resistance (ΔC_F) of a ship's hull due to fouling. The design of experiments (DOE) method was used, followed by factor code translations via nonlinear regression and the optimization method. It was found that some factors and interactions of factors affected the response while others did not. The most influential factor was the roughness height k. Then, the formula was created while still inputting the code of the factor (Equation 9), after which the codes were translated into functions (Equations 10–13) that represented the actual value of each factor. The functions were substituted in Equation 9 to come up with the final alternative formula in Equation 14.

The alternative formula was validated by comparing its calculation result with that of the Granville method and computing the error. The results were quite good, with values of R^2 = 0.9988 and y = 0.9672x + 0.1115, as described in Figure 6. The error distribution is illustrated in Figure 7 and shows that 93.9% of the 1,000 data calculated had a ±5% error risk. The possible cause of this error is the less than perfect process of matching functions during the code translation (Figures 4–5). Of course, this equation can be refined further.

We should be grateful for the DOE, followed by the translation of factors, for allowing the creation of a formula that can calculate a response with good accuracy using minimal initial data. The initial data were generally obtained from measurements in the field, laboratory tests, or numerical simulations, all of which required resources. The resulting formula was also quite easy to use.

Using this alternative formula, predicting the increased frictional resistance of ships due to fouling will be easier, faster, and cheaper. The formula's error rate, which the author considers still quite good, makes the formula suitable as an initial tool for determining how much impact fouling has on ship performance. In addition, this formula has considerable flexibility in the type of roughness function it can be applied to because of its roughness constant variable C_S. The roughness constant is known to be needed because roughness (especially due to biofouling) is very diverse and even random, so it must be represented not only by the measuring height (k) but also by other factors (such as the density, shape, and concavity). Although the values of k and C_S are not easy to determine in the field case, Chung et al. (2021) can provide insights on how to do it. By predicting the impact of biofouling, it is hoped that all parties involved in maritime activities can anticipate and address problems that arise from it.

Acknowledgements

This research project was supported by the Ministry of Research, Technology, and National Innovation and Research Agency (Kemenristek – BRIN) of the Republic of Indonesia under Master to Doctorate Program for Excellent Graduate (PMDSU) scholarship program batch III (Contract No. 1277/PKS/ITS/2020).

References

Abar, I.A.C., Utama, I.K.A.P., 2019. Effect of the Incline Angle of Propeller Boss Cap Fins (PBCF) on Ship Propeller Performance. *International Journal of Technology*, Volume 10(5), pp. 1056–1064

Andersson, J., Oliveira, D.R., Yeginbayeva, I., Leer-Andersen, M., Bensow, R.E., 2020. Review and Comparison of Methods to Model Ship Hull Roughness. *Applied Ocean Research*, Volume 99, https://doi.org/10.1016/j.apor.2020.102119

Atencio, B.N., Chernoray, V., 2019. A Resolved RANS CFD Approach for Drag Characterization of Antifouling Paints. *Ocean Engineering*, Volume 171, pp. 519–532

Bowden, B.., Davison, N.J., 1974. Resistance Increments Due to Hull Roughness Associated with Form Factor Extrapolation Methods. *National Physical Laboratory (NP) Ship Technical Manual 3800*

Cebeci, T., Bradshaw, P., 1977. *Momentum Transfer in Boundary Layers*. Hemisphere Publishing Corporation, New York

Chung, D., Hutchins, N., Schultz, M.P., Flack, K.A., 2021. Predicting the Drag of Rough Surfaces. *Annual Review of Fluid Mechanics*, Volume 53(1), pp. 439–471

Demirel, Y.K., Song, S., Turan, O., Incecik, A., 2019. Practical Added Resistance Diagrams to Predict Fouling Impact on Ship Performance. *Ocean Engineering*, Volume 186, https://doi.org/10.1016/j.oceaneng.2019.106112

Demirel, Y.K., Turan, O., Incecik, A., 2017a. Predicting the Effect of Biofouling on Ship Resistance Using CFD. *Applied Ocean Research*, Volume 62, pp. 100–118

Demirel, Y.K., Uzun, D., Zhang, Y., Fang, H.C., Day, A.H., Turan, O., 2017b. Effect of Barnacle Fouling on Ship Resistance and Powering. *Biofouling*, Volume 33(10), pp. 819–834

Granville, P., 1958. The Frictional Resistance and Turbulent Boundary Layer of Rough Surfaces. *Journal of Ship Research*, Volume 2, pp. 52–74

Granville, P.S., 1987. Three Indirect Methods for the Drag Characterization of Arbitrarily Rough Surfaces on Flat Plates. *Journal of Ship Research*, Volume 31, pp. 70–77

Grigson, C., 1992. Drag Losses of New Ships Caused by Hull Finish. *Journal of Ship Research*, Volume 36(2), pp. 182–196

Hakim, M.L., Nugroho, B., Chin, R.C., Putranto, T., Suastika, I.K., Utama, I.K.A.P., 2020. Drag Penalty Causing from the Roughness of Recently Cleaned and Painted Ship Hull using RANS CFD. *CFD Letters*, Volume 12(3), pp. 78–88

Hakim, M.L., Nugroho, B., Nurrohman, M.N., Suastika, I.K., Utama, I.K.A.P., 2019. Investigation of Fuel Consumption on an Operating Ship Due to Biofouling Growth and Quality of Anti-fouling Coating. *IOP Conference Series: Earth and Environmental Science*, Volume 339, pp. 1–10

Hinkelmann, K., 2012. Design and Analysis of Experiments*. Wiley Series in Probability and Statistics*. John Wiley & Sons, Inc., Hoboken, NJ, USA

Islam, M.F., Lye, L.M., 2009. Combined Use of Dimensional Analysis and Modern Experimental Design Methodologies in Hydrodynamics Experiments. *Ocean Engineering*, Volume 36, pp. 237–247

Jelly, T.O., Busse, A., 2018. Reynolds and Dispersive Shear Stress Contributions above Highly Skewed Roughness. *Journal of Fluid Mechanics*, Volume 852, pp. 710–724

Lasdon, L.S., Waren, A.D., Jain, A., Ratner, M., 1978. Design and Testing of a Generalized Reduced Gradient Code for Nonlinear Programming. *ACM Transactions on Mathematical Software (TOMS)*, Volume 4, pp. 34–50

Lye, L.M., 2002. Design of Experiments in Civil Engineering: Are We Still in the 1920s? *In:* Proceedings, Annual Conference - Canadian Society for Civil Engineering, Montreal, Canada

Molland, A.F., Turnock, S.R., Hudson, D.A., Utama, I.K.A.P., 2014. Reducing Ship Emissions: A Review of Potential Practical Improvements in the Propulsive Efficiency of Future Ships. *Transactions of the Royal Institution of Naval Architects Part A: International Journal of Maritime Engineering*, Volume 156(A2), pp. 175–188

Monty, J.P., Dogan, E., Hanson, R., Scardino, A.J., Ganapathisubramani, B., Hutchins, N., 2016. An Assessment of the Ship Drag Penalty Arising from Light Calcareous Tubeworm Fouling. *Biofouling*, Volume 32, pp. 451–464

Nikuradse, J., 1933. Laws of Flow in Rough Pipes. *NACA Technical Memorandum* 1292

Schoenherr, K.E., 1932. Resistance of Flat Surfaces. *Trans SNAME*, Volume 40, pp. 279–313

Schultz, M.P., 2007. Effects of Coating Roughness and Biofouling on Ship Resistance and Powering. *Biofouling*, Volume 23, pp. 331–341

Schultz, M.P., 2004. Frictional Resistance of Antifouling Coating Systems. *Journal of Fluids Engineering*, Volume 126, pp. 1039–1047

Schultz, M.P., Bendick, J.A., Holm, E.R., Hertel, W.M., 2011. Economic Impact of Biofouling on a Naval Surface Ship. *Biofouling*, Volume 27, pp. 87–98

Schultz, M.P., Flack, K.A., 2007. The Rough-wall Turbulent Boundary Layer from the Hydraulically Smooth to the Fully Rough Regime. *Journal of Fluid Mechanics*, Volume 580, pp. 381–405

Speranza, N., Kidd, B., Schultz, M.P., Viola, I.M., 2019. Modelling of Hull Roughness. *Ocean Engineering*, Volume 174(2), pp. 31–42

Suastika, I.K., Hakim, M.L., Nugroho, B., Nasirudin, A., Utama, I.K.A.P., Monty, J.P., Ganapathisubramani, B., 2021. Characteristics of Drag Due to Streamwise Inhomogeneous Roughness. *Ocean Engineering*, Volume 223, https://doi.org/10.1016/j.oceaneng.2021.108632

Suastika, K., Hidayat, A., Riyadi, S., 2017. Effects of the Application of a Stern Foil on Ship Resistance: A Case Study of an Orela Crew Boat. *International Journal of Technology*, Volume 8(7), pp. 1266–1275

Sulistyawati, W., Suranto, P.J., 2020. Achieving Drag Reduction with Hullform Improvement in Different Optimizing Methods. *International Journal of Technology*, Volume 11(7), pp. 1370–1379

Townsin, R.L., 2003. The Ship Hull Fouling Penalty. *Biofouling*, Volume 19, pp. 9–15

Townsin, R.L., Byrne, D., Svensen, T.E., Milne, A., 1982. Estimating the Technical and Economic Penalties of Hull and Propeller Roughness. *Transactions - Society of Naval Architects and Marine Engineers*, Volume 89, pp. 295–318

Ulman, A., Ferrario, J., Forcada, A., Seebens, H., Arvanitidis, C., Occhipinti-Ambrogi, A., Marchini, A., 2019. Alien Species Spreading via Biofouling on Recreational Vessels in the Mediterranean Sea. *Journal of Applied Ecology*, Volume 56, pp. 2620–2629

Utama, I.K.A.P., Nugroho, B., Nurrohman, M.N., Yusim, A.K., Hakim, M.L., Prasetyo, F.A., Yusuf, M., Suastika, I.K., Ganapathisubramani, B., Monty, J.P., Hutchins, N., 2018. Skin-Friction Drag Measurement over a Recently Cleaned and Painted Ship Hull under Steady Cruising via in-Situ Laser-based Measurement Coupled with Empirical Estimation. *In:* RINA International Conference: Full-scale Ship Performance, RINA HQ, London, pp. 24–25

Yeginbayeva, I.A., Atlar, M., 2018. An Experimental Investigation into the Surface and Hydrodynamic Characteristics of Marine Coatings with Mimicked Hull Roughness Ranges. *Biofouling*, Volume 34, pp. 1001–1019